

CASCADE  $\gamma$ -DECAY OF THE  $^{193}\text{Os}$  COMPOUND NUCLEUS AND SOME  
ASPECTS OF DYNAMICS OF CHANGE IN NUCLEAR PROPERTIES  
BELOW  $B_n$

VALERY A. BONDARENKO<sup>a</sup>, JAROSLAV HONZÁTKO<sup>b</sup>, VALERY A. KHITROV<sup>c</sup>,  
ANATOLY M. SUKHOVOJ<sup>c</sup> and IVO TOMANDL<sup>b</sup>

<sup>a</sup>*Nuclear Research Center, Institute of Solid State Physics, University of Latvia,  
LV 2169 Salaspils, Latvia*

<sup>b</sup>*Nuclear Physics Institute, CZ-25068 Řež near Prague, Czech Republic*

<sup>c</sup>*Frank Laboratory of Neutron Physics, Joint Institute for Nuclear Research, 141980  
Dubna, Russia*

Received 30 January 2002; Accepted 6 September 2002  
Online 7 Februay 2003

Two-step cascades from the  $^{192}\text{Os}(n_{\text{th}}, \gamma)^{193}\text{Os}$  reaction were studied in a  $\gamma - \gamma$  coincidence measurement with two HPGe detectors. The decay scheme of  $^{193}\text{Os}$  was established up to the excitation energy of about 3 MeV. The excitation spectrum of intermediate levels of most intense cascades was found to be practically harmonic.

PACS numbers: 25.40.Lw, 27.80.+w

UDC 539.172.4

Keywords:  $^{192}\text{Os}(n_{\text{th}}, \gamma)^{193}\text{Os}$  reaction, two-step  $\gamma$ -cascades, decay scheme of  $^{193}\text{Os}$

## 1. Introduction

Nuclear properties in the excitation interval up to the neutron binding energy  $B_n$  undergo a radical change: the simplest low-lying levels transform into the Bohr's compound states. The only possibility to study this process in details is provided by the experimental investigation of the two-step  $\gamma$ -cascades proceeding between the neutron resonance and a group of low-lying levels. Experimental data on the density and probability of population of the states observed in this process are compared with the theoretical models. The comparison allows one to reveal the main peculiarities of the change in the properties of nuclear matter as the excitation energy increases. Main details of the analysis of this experiment are described in Refs. [1-3].

## 2. Experiment

Two-step  $\gamma$ -cascades following thermal neutron capture in  $^{190}\text{Os}$  and  $^{192}\text{Os}$  were studied by  $\gamma$ - $\gamma$  coincidence measurements undertaken at the LWR-15 reactor in Rež. The measurements were performed using the spectrometer [4] consisting of two HPGe detectors with the efficiency 20% and 30%. The target consisting of 1200 mg of  $^{192}\text{Os}$  and 176 mg of  $^{190}\text{Os}$  was used. As the thermal neutron capture cross section [5] equals  $13.1 \times 10^{-28} \text{ m}^2$  for  $^{190}\text{Os}$  and  $3.12 \times 10^{-28} \text{ m}^2$  for  $^{192}\text{Os}$ , this target provided 38% of captures in  $^{190}\text{Os}$  and 62% in  $^{192}\text{Os}$ .

Unlike other known methods for the study of the process of thermal neutron capture, the sum coincidence method allows one to obtain very reliable information not only for a monoisotopic target but also for the case of a few isotopes with comparable probabilities of neutron capture in them. In the latter case, the quality of the experimental data is somewhat worse due to:

(a) larger Compton background under the full energy peak in the sum-coincidence spectrum caused by higher-energy cascades belonging to another isotope;

(b) possible overlapping of peaks in the sum coincidence spectrum.

However, a sufficiently high efficiency of detectors and fine energy resolution ( $FWHM \simeq 5 \text{ keV}$  for peaks at  $E_c = 5 - 6 \text{ MeV}$  in the sum-coincidence spectrum) allowed us to obtain the results of acceptable quality also in the present case.

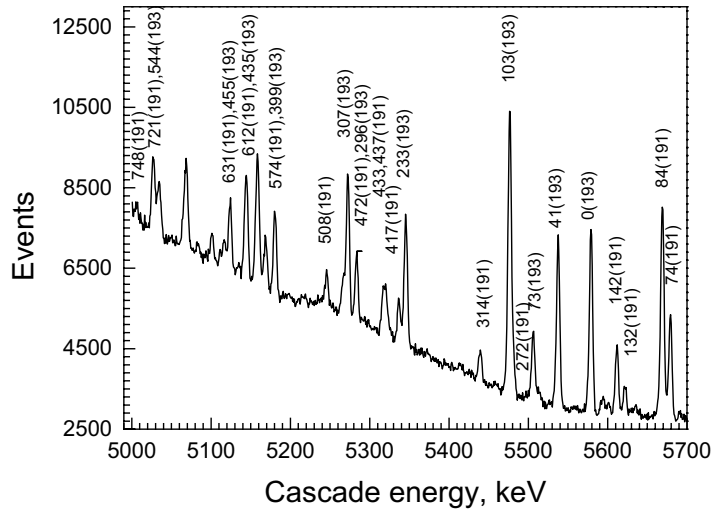


Fig. 1. The part of the sum-coincidence spectrum for  $^{191,193}\text{Os}$ . The peaks are labelled with the energy (in keV) of the final cascade levels. The mass of the corresponding isotope is given in the brackets.

The main part of the sum coincidence spectrum measured in the experiment is shown in Fig. 1. A relatively large background under the peaks in the region of the

neutron binding energy,  $B_n$ , is caused by a parasitic neutron capture in  $\simeq 3$  mg of Cl contained in the target and surrounding constructions. This component of the background, and Compton background at the lower cascade energy  $E_c = E_1 + E_2$ , determine the amplitude and shape of the “noise” line in the intensity distributions of cascades with  $E_c = \text{const}$ . In all, there were obtained and analysed 11 such spectra of cascades in  $^{193}\text{Os}$ . Each two-step cascade in such a spectrum is presented by a pair of peaks with equal areas and widths [6]. The probability of observing a low-intensity cascade is determined only by the amplitude of the “noise” line. The registration threshold,  $L_c$ , for individual cascades was determined from an analysis of spectra  $E_c = \text{const}$  corresponding to the background intervals in the sum-coincidence spectrum. It was established that  $L_c$  linearly increases from 1.5 to 6.0 events per  $10^4$  decays as the cascade energy changes from 5.6 to 4.5 MeV.

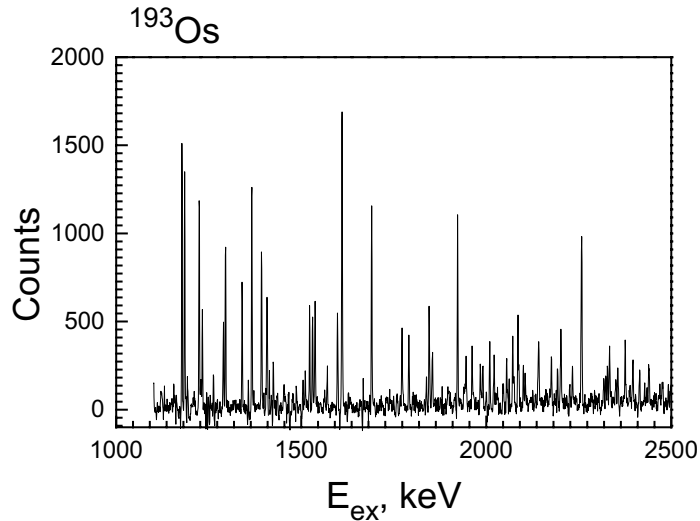


Fig. 2. Part of the intensity distribution of the two-step cascades summed over 11 cascade final levels in  $^{193}\text{Os}$ .

The data obtained allow one to clearly demonstrate spectroscopic possibilities of the method. To show this, all 11 intensity distributions of cascades observed were summed. The part of the summed spectrum for the interval of the quantum energy  $E_\gamma$  from 3.0 to 4.6 MeV is presented in Fig. 2 as a function of the energy  $E_{ex} = B_n - E_\gamma$  ( $E_{ex}$  equals excitation energy of the cascade intermediate level, while  $E_\gamma$  is the energy of the cascade primary transition  $E_1$ ). Summation leads to the accumulation of the primary transition intensities in the common peak, and of intensities of the secondary transitions – in different peaks. Due to the low intensity, the cascades with the secondary transition energy  $E_2 > 3$  MeV are not observed in a given interval of the excitation energy as the peaks, i.e., they form continuous distribution. Therefore, every peak in Fig. 2 with the high probability corresponds to one of the levels of  $^{193}\text{Os}$ . So, one can see from Fig. 2 that our experimental data allow confident determination of the level energies in  $^{193}\text{Os}$  at least up to  $0.5B_n$ , even without the use of the most modern spectrometers.

### 3. Spectroscopic information

The method of construction of a decay scheme using the obvious assumption about the constancy of the energy  $E_1 = B_n - E_m$  of the primary transition in the cascades with the different total energy  $E_1 + E_2 = \text{const}$  was described for the first time in Ref. [7]. The method uses the multi-dimensional distribution in the framework of the maximum likelihood method in order to select probable  $\gamma$ -transitions with equal energy in different spectra. The algorithm gives reliable results [8] even with the mean error in the determination of  $E_1$  up to about 1.5 keV, and the number of cascades resolved in the spectrum as pairs of peaks of about  $10^3$ . Corresponding results for  $^{193}\text{Os}$  are given in Table 1.

TABLE 1. A list of absolute intensities (per  $10^2$  decays),  $i_{\gamma\gamma}$ , of measured two-step cascades, and energies,  $E_1$  and  $E_2$ , of the cascade transitions.  $E_i$  are the energies of intermediate levels. Only statistical uncertainties of determination of energies and intensities are given (in parentheses). The lower estimates of  $i_{\gamma\gamma}$  for cascades with  $E_1 < 520$  keV or  $E_2 < 520$  keV are listed. All energies are in keV.

$E_1$	$E_i$	$E_2$	$i_{\gamma\gamma}$	$E_1$	$E_i$	$E_2$	$i_{\gamma\gamma}$
5277.00	306.90 (10)	306.90	0.326 (16)			1105.40	0.107 (8)
		265.42	2.209 (52)			1075.57	0.342 (11)
		204.17	0.374 (13)			871.22	0.097 (15)
5033.00	550.90 (20)	448.17	0.032 (4)			779.28	0.020 (7)
5010.70	573.20 (20)	266.12	0.055 (12)			722.53	0.131 (9)
4996.30	587.60 (10)	353.74	0.041 (6)	4398.50	1185.40 (20)	1082.67	0.023 (6)
4908.70	675.20 (10)	633.72	0.017 (4)	4378.70	1205.20 (50)	1163.72	0.076 (9)
		572.47	0.013 (4)			1102.47	0.097 (6)
4795.40	788.50 (10)	788.50	0.025 (5)	4366.40	1217.50 (26)	1217.50	0.176 (9)
4694.50	889.40 (10)	889.40	1.031 (19)			1176.02	0.593 (21)
		847.92	0.087 (9)			1144.60	0.090 (8)
		816.50	0.165 (8)			1114.77	0.433 (13)
		786.67	0.821 (27)			921.82	0.024 (7)
		655.54	0.183 (16)			910.42	0.066 (12)
		582.32	0.207 (45)			818.48	0.094 (10)
4617.00	966.90 (18)	671.22	0.014 (4)			761.73	0.072 (6)
		567.88	0.011 (3)	4358.20	1225.70 (41)	1184.22	0.026 (6)
4530.20	1053.70 (20)	1053.70	0.312 (8)			1152.80	0.020 (6)
		1012.22	0.688 (15)			769.93	0.448 (16)
		980.80	0.065 (5)	4339.30	1244.60 (39)	1203.12	0.015 (6)
		950.97	5.791 (49)			788.83	0.062 (6)
		746.62	0.500 (38)	4316.60	1267.30 (27)	1164.57	0.093 (10)
4499.40	1084.50 (45)	1043.02	0.033 (4)	4301.00	1282.90 (20)	1282.90	0.170 (9)
		788.82	0.070 (9)			1241.42	0.100 (6)
4413.20	1170.70 (40)	1170.70	0.097 (8)			1210.00	0.036 (4)
		1129.22	0.806 (24)			1180.17	0.068 (8)
		1097.80	0.171 (10)			987.22	0.032 (7)
		1067.97	0.226 (10)			883.88	0.119 (14)
		936.84	0.176 (16)	4295.30	1288.60 (10)	573.70	0.031 (6)
		875.02	0.161 (12)			1288.60	0.630 (18)
		863.62	0.034 (11)			1247.12	0.127 (6)
		714.93	0.030 (6)			1215.70	0.014 (4)
		461.50	0.083 (7)			1185.87	0.040 (8)
4405.60	1178.30 (20)	1178.30	0.717 (19)			992.92	0.064 (7)
		1136.82	0.029 (6)			889.58	0.081 (11)

Table 1. (cont.)

$E_1$	$E_i$	$E_2$	$i_{\gamma\gamma}$	$E_1$	$E_i$	$E_2$	$i_{\gamma\gamma}$
4250.40	1333.50 (30)	579.40	0.063 ( 6)	4028.10	1555.80 (20)	1427.57	0.327 (13)
		399.12	0.115 (12)			1234.62	0.037 ( 8)
		1333.50	0.060 ( 5)			1223.22	0.062 ( 6)
		1292.02	0.083 ( 6)			1131.28	0.035 (11)
		1260.60	0.017 ( 4)			1514.32	0.060 ( 6)
		1230.77	0.448 (17)			1248.72	0.035 ( 6)
		1099.64	0.112 (14)			1590.90	0.222 (11)
		1037.82	0.021 ( 7)			1549.42	0.040 ( 5)
		934.48	0.026 ( 9)			1518.00	0.049 ( 5)
		877.73	0.029 (12)			1488.17	0.087 ( 8)
4224.30	1359.60 (30)	1359.60	0.045 ( 5)			1295.22	0.046 ( 6)
		1318.12	0.059 ( 5)			1283.82	0.139 (12)
		1286.70	0.035 ( 4)			1603.20	0.046 ( 6)
		1256.87	0.108 (10)			1561.72	0.671 (17)
		1125.74	0.851 (37)			1530.30	0.023 ( 5)
		1063.92	0.047 ( 5)			1500.47	0.610 (17)
		1052.52	0.065 ( 6)			1369.34	0.029 ( 6)
		960.58	0.144 (15)			1307.52	0.178 (10)
		903.83	0.095 (14)			1296.12	0.272 (16)
		1076.52	0.029 ( 6)			1204.18	0.212 (16)
4197.90	1383.60 (30)	1386.00	0.754 (18)			1147.43	0.155 (14)
		1344.52	0.140 ( 9)			1618.82	0.017 ( 5)
		1313.10	0.029 ( 5)			1680.30 (42)	0.024 ( 8)
		1283.27	0.019 ( 4)			3900.60	1683.30 (17)
		1090.32	0.027 ( 5)			1641.82	0.350 (12)
		1078.92	0.096 ( 7)			1610.40	0.021 ( 5)
		1398.20	0.069 ( 8)			1580.57	0.445 (15)
		1325.30	0.032 ( 5)			1449.44	0.250 (12)
		1400.00	0.034 ( 6)			1387.62	0.138 ( 9)
		1358.52	0.017 ( 6)			1376.22	0.072 ( 9)
4185.70	1398.20 (36)	1297.27	0.199 ( 8)			974.10	0.042 ( 6)
		1092.92	0.043 ( 6)			3861.40	1722.50 (30)
		1418.00	0.066 ( 6)			1722.50	0.019 ( 5)
		1376.52	0.016 ( 5)			1619.77	0.017 ( 6)
		1345.10	0.045 ( 5)			1426.82	0.018 ( 6)
		1122.32	0.022 ( 5)			3852.30	1731.60 (33)
		1434.00	0.014 ( 5)			842.12	0.058 ( 9)
		1446.50 (57)	0.112 ( 6)			3846.30	1737.60 (60)
		1373.60	0.012 ( 5)			3839.00	1744.90 (90)
		1497.40 (45)	0.018 ( 5)			1672.00	0.016 ( 5)
4086.50	1497.40 (45)	1504.10	0.024 ( 5)			1289.13	0.016 ( 5)
		1401.37	0.025 ( 6)			3829.70	1754.20 (110)
		1270.24	0.070 ( 6)			1754.20	0.016 ( 5)
		1048.33	0.038 ( 9)			1520.34	0.016 ( 4)
		1515.60(100)	0.021 ( 5)			3823.50	1760.40 (20)
		1474.12	0.051 ( 6)			1657.67	0.047 ( 8)
		1412.87	0.085 ( 8)			3818.80	1765.10 (85)
		1219.92	0.054 ( 8)			1723.62	0.074 ( 6)
		1208.52	0.200 (11)			1692.20	0.027 ( 5)
		1116.58	0.083 (11)			1662.37	0.108 ( 8)
4079.80	1504.10 (41)	1059.83	0.060 (10)			1531.24	0.102 ( 6)
		1523.50	0.069 ( 6)			1458.02	0.117 ( 8)
		1482.02	0.067 ( 6)			1366.08	0.056 ( 5)
		1420.77	0.207 (11)			1309.33	0.048 ( 5)
		1216.42	0.207 (11)			1055.90	0.025 ( 6)
		1530.30 (29)	0.248 (10)			3800.10	1783.80 (90)
		1488.82	0.248 (10)			1783.80	0.065 ( 6)
						1742.32	0.112 ( 7)
						1710.90	0.033 ( 5)
						1549.94	0.129 ( 7)
4068.30						1488.12	0.025 ( 5)

Table 1. (cont.)

$E_1$	$E_i$	$E_2$	$i_{\gamma\gamma}$	$E_1$	$E_i$	$E_2$	$i_{\gamma\gamma}$
		1476.72	0.035 ( 6)	3648.80	1935.10 (16)	1859.20	0.089 ( 5)
		1384.78	0.035 ( 5)			1935.10	0.023 (10)
		1328.03	0.030 ( 5)			1832.37	0.082 ( 6)
3788.10	1795.80 (43)	1693.07	0.021 ( 6)			1536.08	0.023 ( 5)
		1561.94	0.019 ( 4)	3645.30	1938.60 (44)	1938.60	0.321 (24)
3785.00	1798.90 (50)	1565.04	0.030 ( 4)			1897.12	0.048 ( 5)
3781.90	1802.00 (75)	1760.52	0.022 ( 5)	3634.90	1949.00 (42)	1641.92	0.018 ( 6)
3778.80	1805.10 (34)	1805.10	0.026 ( 5)	3629.10	1954.80 (20)	1852.07	0.355 (11)
3757.20	1826.70 (90)	1826.70	0.018 ( 5)			1720.94	0.022 ( 4)
		1753.80	0.014 ( 5)			1647.72	0.016 ( 6)
3752.80	1831.10 (28)	1831.10	0.029 ( 5)			1499.03	0.017 ( 5)
		1789.62	0.037 ( 5)	3606.50	1977.40 (90)	1935.92	0.037 ( 5)
		1758.20	0.032 ( 5)			1743.54	0.030 ( 4)
		1597.24	0.037 ( 4)			1670.32	0.107 ( 8)
		1535.42	0.027 ( 5)			1578.38	0.021 ( 5)
		1524.02	0.018 ( 6)	3600.50	1983.40 (22)	1087.92	0.054 (10)
		1432.08	0.020 ( 4)			1983.40	0.160 (16)
3745.60	1838.30 (20)	1375.33	0.022 ( 5)			1910.50	0.067 ( 5)
		1765.40	0.021 ( 5)			1880.67	0.070 ( 6)
		1735.57	0.025 ( 6)			1749.54	0.015 ( 4)
		1604.44	0.073 ( 5)	3594.10	1989.80 (60)	1687.72	0.020 ( 6)
		1531.22	0.399 (15)	3581.80	2002.10 (28)	1755.94	0.020 ( 4)
3736.80	1847.10 (52)	1129.10	0.051 ( 9)			1960.62	0.210 (11)
		1847.10	0.026 ( 6)			1929.20	0.087 ( 6)
		1805.62	0.065 ( 6)			1768.24	0.048 ( 5)
		1774.20	0.024 ( 5)			1706.42	0.039 ( 6)
		1744.37	0.080 ( 8)			1695.02	0.040 ( 6)
		1551.42	0.019 ( 5)			1603.08	0.025 ( 6)
		1540.02	0.028 ( 6)	3570.30	2013.60 (37)	1972.12	0.123 ( 9)
		1448.08	0.073 ( 5)			1910.87	0.032 ( 6)
		1137.90	0.047 ( 9)			1779.74	0.015 ( 4)
3730.30	1853.60 (92)	1619.74	0.016 ( 4)			1706.52	0.051 ( 6)
3721.20	1862.70 (80)	1759.97	0.029 ( 6)			1557.83	0.017 ( 6)
3709.30	1874.60 (45)	1874.60	0.031 (10)			1124.12	0.094 (10)
3695.00	1888.90 (84)	1816.00	0.029 ( 5)	3563.10	2020.80 (80)	1786.94	0.022 ( 4)
		1786.17	0.032 ( 8)			1713.72	0.021 ( 6)
		1489.88	0.024 ( 5)	3559.60	2024.30 (55)	1982.82	0.027 ( 6)
		1179.70	0.037 ( 9)	3546.50	2037.40 (80)	1803.54	0.030 ( 5)
3691.30	1892.60 (27)	1892.60	0.025 (10)			1741.72	0.022 ( 6)
		1851.12	0.040 ( 5)			1730.32	0.018 ( 5)
		1819.70	0.040 ( 5)			1581.63	0.030 ( 6)
		1436.83	0.021 ( 6)	3544.00	2039.90 (70)	2039.90	0.043 ( 5)
3675.30	1908.60 (35)	1867.12	0.015 ( 5)			1732.82	0.021 ( 5)
		1509.58	0.032 ( 6)	3535.80	2048.10 (30)	2048.10	0.141 ( 8)
		1452.83	0.025 ( 6)			1945.37	0.049 ( 8)
3668.60	1915.30 (43)	1915.30	0.029 (10)			1814.24	0.049 ( 6)
		1873.82	0.411 (12)	3533.10	2050.80 (80)	1741.02	0.040 ( 5)
		1812.57	0.030 ( 6)			1816.94	0.023 ( 5)
		1681.44	0.294 (10)			1755.12	0.046 ( 6)
		1608.22	0.416 (16)	3530.40	2053.50 (85)	1651.78	0.046 ( 5)
		1516.28	0.019 ( 6)	3524.20	2059.70 (20)	1950.77	0.080 (10)
		1459.53	0.022 ( 6)	3519.80	2064.10 (16)	2018.22	0.018 ( 6)
3662.70	1921.20 (30)	1848.30	0.013 ( 5)			2064.10	0.039 ( 5)
		1818.47	0.030 ( 6)			2022.62	0.051 ( 7)
3651.80	1932.10 (60)	1890.62	0.028 ( 5)			1991.20	0.076 ( 6)

Table 1. (cont.)

$E_1$	$E_i$	$E_2$	$i_{\gamma\gamma}$	$E_1$	$E_i$	$E_2$	$i_{\gamma\gamma}$
3516.30	2067.60 ( 8)	1961.37	0.097 (10)	3449.70	2134.20 (40)	1677.23	0.054 ( 6)
		1757.02	0.053 ( 5)			1243.52	0.168 ( 9)
		1665.08	0.059 ( 6)			2134.20	0.021 ( 5)
		1608.33	0.049 ( 6)			1900.34	0.048 ( 6)
		1354.90	0.019 ( 7)			1827.12	0.086 ( 6)
		2067.60	0.030 ( 5)			2040.77	0.015 ( 6)
		1833.74	0.082 ( 6)			2109.12	0.018 ( 7)
		1760.52	0.043 ( 5)			1854.92	0.023 ( 5)
		1178.12	0.052 ( 8)			2051.07	0.061 ( 8)
		2078.30	0.039 ( 5)			1858.12	0.039 ( 5)
3505.60	2078.30 (50)	2036.82	0.295 (12)	3426.80	2157.10 (10)	2157.10	0.030 ( 5)
		2005.40	0.031 ( 5)			1850.02	0.028 ( 5)
		1844.44	0.052 ( 5)			2090.80	0.042 ( 5)
		1782.62	0.020 ( 6)			1929.84	0.026 ( 4)
		1771.22	0.115 ( 7)			1707.93	0.021 ( 6)
		1679.28	0.027 ( 5)			2168.70	0.111 ( 8)
		1622.53	0.043 ( 6)			2127.22	0.187 (11)
		1369.10	0.026 ( 7)			2065.97	0.017 ( 6)
		1188.82	0.032 ( 8)			1873.02	0.023 ( 5)
		2008.20	0.054 ( 5)			1861.62	0.026 ( 5)
3502.80	2081.10 (46)	1978.37	0.042 ( 8)	3405.80	2178.10 (10)	1769.68	0.049 ( 5)
		1785.42	0.027 ( 6)			1288.62	0.042 (11)
		1774.02	0.035 ( 5)			2139.82	0.056 ( 7)
		1682.08	0.052 ( 6)			2108.40	0.019 ( 5)
		1625.33	0.025 ( 6)			2143.92	0.017 ( 6)
		2092.90	0.020 ( 5)			2082.67	0.146 (10)
		2020.00	0.022 ( 5)			1878.32	0.023 (11)
		1990.17	0.038 ( 8)			1295.92	0.048 (11)
		1859.04	0.032 ( 5)			2150.92	0.063 ( 7)
		1797.22	0.038 ( 6)			2089.67	0.078 ( 8)
3491.00	2092.90 (20)	1693.88	0.111 ( 7)	3391.50	2192.40 (22)	1483.20	0.029 ( 8)
		1203.42	0.028 ( 8)			2092.27	0.046 ( 8)
		2098.00	0.024 ( 5)			1887.92	0.216 (19)
		2056.52	0.021 ( 6)			1795.98	0.016 ( 5)
		1995.27	0.021 ( 8)			1305.52	0.082 (11)
		1864.14	0.045 ( 5)			2102.37	0.040 ( 6)
		1802.32	0.023 ( 6)			1806.08	0.018 ( 5)
		1790.92	0.020 ( 5)			2218.60	0.030 ( 5)
		1388.80	0.047 ( 7)			1984.74	0.073 ( 6)
		1208.52	0.045 ( 8)			1922.92	0.033 ( 5)
3480.50	2103.40 (40)	2061.92	0.018 ( 6)			1819.58	0.014 ( 5)
		1807.72	0.018 ( 6)	3361.90	2222.00 (26)	2222.00	0.014 ( 5)
3475.80	2108.10 (80)	1874.24	0.022 ( 6)			1988.14	0.024 ( 5)
3472.20	2111.70 (70)	2111.70	0.024 ( 5)	3358.80	2225.10 (30)	2183.62	0.251 (12)
3468.00	2115.90 (50)	1222.22	0.034 ( 8)	3353.30	2230.60 (28)	1929.42	0.026 ( 5)
3459.80	2124.10 (32)	2074.42	0.032 ( 6)	3349.30	2234.60 (70)	2230.60	0.023 ( 5)
3457.50	2126.40 (32)	2021.37	0.046 ( 8)	3344.00	2239.90 (50)	2127.87	0.042 ( 6)
3450.90	2133.00 (67)	1890.24	0.022 ( 4)	3337.60	2246.30 (70)	2234.60	0.021 ( 5)
		2084.92	0.032 ( 6)	3334.80	2249.10 (20)	2198.42	0.021 ( 6)
		1819.32	0.032 ( 5)			2204.82	0.029 ( 6)
		2133.00	0.030 ( 5)			2176.20	0.152 ( 9)
		2030.27	0.017 ( 6)			2146.37	0.067 ( 8)
		1899.14	0.054 ( 7)			1942.02	0.380 (25)
		1837.32	0.037 ( 5)			1850.08	0.088 ( 7)
		1733.98	0.037 ( 5)			1359.62	0.058 (11)

Table 1. (cont.)

$E_1$	$E_i$	$E_2$	$i_{\gamma\gamma}$	$E_1$	$E_i$	$E_2$	$i_{\gamma\gamma}$
3334.70	2249.20 (95)	1540.00	0.061 (12)	3194.80	2389.10 (43)	1491.52	0.033 (8)
3333.00	2250.90 (70)	2250.90	0.602 (26)			2389.10	0.153 (10)
		2209.42	0.028 (6)			2347.62	0.026 (6)
3328.00	2255.90 (20)	2153.17	0.021 (6)			2286.37	0.055 (6)
		1948.82	0.031 (11)			2155.24	0.020 (5)
3325.50	2258.40 (40)	2258.40	0.024 (9)			2093.42	0.023 (6)
		1859.38	0.022 (5)			1990.08	0.022 (9)
3305.20	2278.70 (20)	2205.80	0.028 (5)			1933.33	0.028 (10)
		2175.97	0.021 (6)			1499.62	0.065 (8)
		1983.02	0.020 (6)	3187.60	2396.30 (31)	2396.30	0.046 (5)
3298.50	2285.40 (40)	2182.67	0.055 (6)	3176.90	2407.00 (47)	2407.00	0.024 (5)
3293.40	2290.50 (30)	2290.50	0.020 (8)			2365.52	0.072 (6)
		2249.02	0.033 (5)			2304.27	0.080 (8)
3289.60	2294.30 (31)	2294.30	0.021 (8)			2111.32	0.041 (7)
3286.60	2297.30 (60)	2255.82	0.032 (5)			2007.98	0.031 (9)
		2224.40	0.033 (5)	3169.90	2414.00 (85)	2372.52	0.021 (6)
		2194.57	0.017 (6)	3162.90	2421.00 (27)	2379.52	0.070 (7)
3273.90	2310.00 (15)	2310.00	0.052 (14)			2021.98	0.017 (5)
		2268.52	0.045 (5)	3157.10	2426.80 (40)	2426.80	0.055 (6)
		2076.14	0.035 (16)			2324.07	0.036 (6)
3268.00	2315.90 (78)	2315.90	0.026 (9)			2192.94	0.017 (5)
		2274.42	0.056 (5)	3152.60	2431.30 (80)	2431.30	0.047 (6)
		2020.22	0.022 (6)			2328.57	0.093 (10)
		2008.82	0.020 (8)	3151.10	2432.80 (40)	2432.80	0.019 (5)
3263.40	2320.50 (27)	2320.50	0.107 (13)			2391.32	0.155 (9)
		2217.77	0.076 (6)			2330.07	0.019 (8)
		2086.64	0.078 (7)			2125.72	0.037 (9)
		2024.82	0.020 (6)			2033.78	0.019 (5)
3257.80	2326.10 (90)	2326.10	0.066 (10)	3146.20	2437.70 (40)	2396.22	0.017 (6)
		2284.62	0.048 (5)	3141.40	2442.50 (52)	2442.50	0.032 (5)
		2223.37	0.291 (11)	3136.90	2447.00(100)	2405.52	0.051 (6)
		2030.42	0.027 (6)			2151.32	0.019 (6)
3251.30	2332.60 (29)	2291.12	0.016 (5)	3133.80	2450.10 (55)	2377.20	0.015 (5)
		2229.87	0.017 (6)			2347.37	0.019 (6)
3243.80	2340.10 (42)	2298.62	0.026 (5)	3125.40	2458.50 (20)	2355.77	0.027 (6)
3241.00	2342.90 (80)	2301.42	0.029 (5)			2151.42	0.017 (6)
		2240.17	0.055 (6)	3122.20	2461.70 (50)	2461.70	0.027 (5)
3235.90	2348.00 (24)	2348.00	0.032 (5)			2227.84	0.110 (7)
		2306.52	0.110 (6)	3116.20	2467.70 (50)	2154.62	0.031 (6)
		2245.27	0.055 (6)			2426.22	0.052 (6)
		2114.14	0.029 (6)			2364.97	0.021 (6)
3233.50	2350.40 (40)	2043.32	0.019 (8)			2233.84	0.022 (5)
3223.00	2360.90 (75)	2127.04	0.021 (6)			2160.62	0.019 (6)
3219.70	2364.20 (37)	2364.20	0.024 (5)			2068.68	0.020 (5)
		2261.47	0.025 (6)			2011.93	0.025 (10)
3215.90	2368.00 (29)	2326.52	0.052 (6)	3113.50	2470.40 (29)	2470.40	0.025 (8)
		2265.27	0.093 (8)			2163.32	0.025 (6)
		2134.14	0.172 (11)	3099.60	2484.30 (20)	2442.82	0.057 (6)
		2060.92	0.019 (8)			2381.57	0.023 (6)
		1478.52	0.064 (8)			2250.44	0.035 (5)
3210.80	2373.10 (34)	2373.10	0.016 (5)	3097.20	2486.70 (65)	2179.62	0.016 (6)
3202.90	2381.00 (27)	2381.00	0.043 (5)	3094.30	2489.60 (25)	2489.60	0.044 (6)
		2308.10	0.019 (5)			2386.87	0.021 (8)
		2073.92	0.020 (8)			2182.52	0.024 (6)

Table 1. (cont.)

$E_1$	$E_i$	$E_2$	$i_{\gamma\gamma}$	$E_1$	$E_i$	$E_2$	$i_{\gamma\gamma}$
3088.90	2495.00 (70)	2090.58	0.033 ( 5)	3023.50	2558.10 (44)	2516.62	0.081 ( 7)
		2422.10	0.070 ( 5)			2251.02	0.022 ( 6)
		2261.14	0.015 ( 5)			2487.50	0.030 ( 5)
		2187.92	0.024 ( 5)			2457.67	0.030 ( 8)
		2039.23	0.063 ( 7)			2326.54	0.035 ( 5)
		2499.70	0.027 ( 6)			2253.32	0.040 ( 6)
		2458.22	0.077 ( 15)			2567.10	0.070 ( 9)
		2426.80	0.027 ( 5)			2525.62	0.040 ( 6)
		2396.97	0.021 ( 8)			2494.20	0.057 ( 6)
		2265.84	0.025 ( 5)			2260.02	0.042 ( 6)
3080.40	2503.50 (32)	2204.02	0.051 ( 6)			2168.08	0.034 ( 6)
		2503.50	0.019 ( 6)			2111.33	0.047 ( 6)
		2506.30(100)	0.045 ( 5)			2344.14	0.027 ( 9)
		2508.30	0.083 ( 8)			2538.62	0.032 ( 6)
		2466.82	0.034 ( 7)			2507.20	0.045 ( 5)
		2405.57	0.027 ( 8)			2477.37	0.158 (10)
		2274.44	0.073 ( 6)			2346.24	0.052 ( 9)
		2201.22	0.022 ( 5)			2284.42	0.024 ( 6)
		2109.28	0.020 ( 5)			2124.33	0.037 ( 6)
		2052.53	0.044 ( 6)	3005.90	2585.00 (85)	2585.00	0.018 ( 6)
3072.10	2511.80 (70)	2511.80	0.031 ( 6)			2543.52	0.030 ( 6)
		2438.90	0.040 ( 5)			2597.40	0.067 ( 9)
		2409.07	0.070 (10)			2363.54	0.019 ( 5)
		2204.72	0.023 ( 6)			2602.80	0.021 ( 6)
		2112.78	0.086 ( 6)			2561.32	0.029 ( 7)
		2056.03	0.028 ( 6)			2529.90	0.043 ( 5)
		2514.10	0.026 ( 6)			2203.78	0.028 ( 6)
		2472.62	0.023 ( 7)			2147.03	0.022 ( 6)
		2280.24	0.039 ( 5)	2977.00	2606.90 (32)	2504.17	0.023 ( 6)
		2218.42	0.020 ( 6)			2611.30	0.020 ( 6)
3064.70	2519.20 (50)	2207.02	0.027 ( 6)			2569.82	0.233 (13)
		2519.20	0.032 ( 6)			2508.57	0.049 ( 6)
		2477.72	0.032 ( 7)			2315.62	0.048 ( 6)
		2446.30	0.018 ( 5)			1902.10	0.030 ( 8)
		2416.47	0.034 ( 8)			2380.84	0.028 ( 5)
		2063.43	0.035 ( 6)			2526.57	0.044 ( 6)
		2528.40	0.015 ( 6)			2322.22	0.015 ( 6)
		2455.50	0.030 ( 5)			2632.30	0.049 ( 8)
		2425.67	0.019 ( 8)			2590.82	0.041 ( 7)
		2072.63	0.026 ( 6)			2529.57	0.030 ( 6)
3053.00	2530.90 (40)	2223.82	0.021 ( 6)	2946.10	2637.80 (30)	2637.80	0.018 ( 6)
		2533.70	0.105 ( 9)			2596.32	0.039 ( 6)
		2299.84	0.058 ( 5)			2535.07	0.015 ( 6)
		2541.80	0.015 ( 6)			2656.60	0.043 ( 6)
		2468.90	0.022 ( 6)			2615.12	0.057 ( 7)
		2439.07	0.076 (10)			2553.87	0.040 ( 8)
		2307.94	0.052 ( 5)			2661.80	0.020 ( 6)
		2234.72	0.051 ( 6)			2671.40	0.125 (11)
		2086.03	0.051 ( 6)			2629.92	0.077 ( 7)
		2445.47	0.044 ( 8)			2598.50	0.040 ( 6)
3035.70	2548.20 (60)	2314.34	0.093 ( 6)			2568.67	0.057 (11)
		2252.52	0.029 ( 7)			2437.54	0.035 ( 6)
		2551.30	0.144 (10)			2364.32	0.060 ( 6)
		2554.60	0.016 ( 6)			2679.60	0.030 ( 8)
		2247.52	0.019 ( 6)			2638.12	0.035 ( 6)

Table 1. (cont.)

$E_1$	$E_i$	$E_2$	$i_{\gamma\gamma}$	$E_1$	$E_i$	$E_2$	$i_{\gamma\gamma}$
		2445.74	0.022 ( 6)	2825.70	2758.20 (29)	2524.34	0.044 ( 6)
		2280.58	0.072 ( 6)	2822.20	2761.70 (85)	2761.70	0.030 ( 6)
2896.80	2687.10 (14)	2645.62	0.032 ( 6)	2819.00	2764.90 (30)	2457.82	0.026 ( 6)
		2614.20	0.026 ( 6)	2810.00	2773.90 (30)	2773.90	0.040 ( 6)
2893.70	2690.20 (35)	2648.72	0.028 ( 6)			2732.42	0.018 ( 6)
		2456.34	0.033 ( 7)			2671.17	0.070 ( 8)
2890.00	2693.90 (52)	2621.00	0.026 ( 6)			2540.04	0.022 ( 6)
		2591.17	0.019 ( 6)			2466.82	0.033 ( 6)
2886.90	2697.00 (50)	2594.27	0.047 ( 8)	2804.50	2779.40 (30)	2545.54	0.018 ( 6)
		2463.14	0.030 ( 7)	2801.80	2782.10 (38)	2782.10	0.025 ( 6)
		2401.32	0.051 ( 8)			2740.62	0.023 ( 6)
		2389.92	0.019 ( 6)			2709.20	0.032 ( 6)
2884.40	2699.50 (70)	2699.50	0.076 ( 8)			2679.37	0.030 ( 6)
		2658.02	0.041 ( 7)			2548.24	0.029 ( 9)
		2626.60	0.024 ( 6)			2475.02	0.023 ( 6)
		2596.77	0.101 (10)	2799.80	2784.10 (44)	2326.33	0.026 ( 7)
		2465.64	0.024 ( 7)			2550.24	0.027 ( 9)
		2300.48	0.026 ( 5)			2477.02	0.041 ( 6)
2880.20	2703.70 (75)	2662.22	0.046 ( 7)	2791.90	2792.00 (23)	2750.52	0.015 ( 6)
		2600.97	0.032 ( 8)			2496.32	0.024 ( 7)
		2469.84	0.076 ( 9)	2786.00	2797.90 (45)	2484.92	0.049 ( 6)
		2396.62	0.045 ( 6)			2797.90	0.037 ( 6)
		2304.68	0.016 ( 5)			2695.17	0.087 ( 8)
2875.00	2708.90 (65)	2475.04	0.066 ( 8)			2564.04	0.022 ( 6)
		2413.22	0.022 ( 7)			2490.82	0.039 ( 6)
2869.10	2714.80 (14)	2480.94	0.022 ( 6)	2778.40	2805.50 (85)	2805.50	0.027 ( 6)
		2407.72	0.032 ( 6)			2764.02	0.082 ( 7)
2867.00	2716.90 (42)	2409.82	0.029 ( 6)			2702.77	0.072 ( 6)
2863.70	2720.20 (60)	2720.20	0.025 ( 6)			2349.73	0.032 ( 6)
		2678.72	0.057 (12)	2772.30	2811.60 (60)	2738.70	0.024 ( 6)
		2647.30	0.026 ( 6)			2504.52	0.029 ( 6)
		2486.34	0.026 ( 6)	2761.10	2822.80 (19)	2113.60	0.030 ( 7)
		2413.12	0.028 ( 6)	2753.60	2830.30 (45)	2727.57	0.036 ( 6)
		2321.18	0.021 ( 5)			2596.44	0.097 ( 7)
		2264.43	0.024 ( 7)	2749.60	2834.30 (60)	2731.57	0.042 ( 6)
2860.30	2723.60 (36)	2650.70	0.023 ( 6)	2727.60	2856.30 (50)	2856.30	0.138 ( 9)
		2489.74	0.048 ( 6)			2753.57	0.036 ( 6)
2855.70	2728.20 (52)	2686.72	0.057 ( 7)			2549.22	0.032 ( 6)
		2625.47	0.029 ( 6)	2720.10	2863.80 (17)	2822.32	0.041 ( 6)
2851.80	2732.10 (42)	2732.10	0.062 (11)			2761.07	0.055 ( 6)
2849.60	2734.30 (18)	2734.30	0.062 (10)			2408.03	0.082 ( 7)
		2500.44	0.027 ( 6)			2154.60	0.045 ( 7)
2845.50	2738.40 (40)	2696.92	0.018 (10)	2713.90	2870.00 (22)	2870.00	0.071 ( 8)
		2635.67	0.021 ( 8)			2828.52	0.099 ( 9)
		2504.54	0.021 ( 6)			2767.27	0.190 (10)
2842.00	2741.90 (20)	2741.90	0.056 ( 6)	2708.10	2875.80 (40)	2875.80	0.045 ( 6)
		2639.17	0.030 ( 8)			2773.07	0.019 ( 6)
		2508.04	0.020 ( 6)			2641.94	0.020 ( 6)
		2434.82	0.021 ( 6)	2703.90	2880.00 (44)	2807.10	0.027 ( 6)
2837.20	2746.70 (12)	2643.97	0.053 ( 8)			2646.14	0.025 ( 6)
2834.10	2749.80 (22)	2749.80	0.025 ( 6)	2696.90	2887.00 (61)	2814.10	0.127 ( 9)
		2676.90	0.056 ( 6)			2579.92	0.019 ( 6)
		2647.07	0.038 ( 8)			2487.98	0.028 ( 6)
2831.00	2752.90 (36)	2519.04	0.016 ( 6)	2679.80	2904.10 (47)	2597.02	0.034 ( 6)
		2445.82	0.027 ( 6)	2674.90	2909.00 (92)	2909.00	0.026 ( 8)

Table 1. (cont.)

$E_1$	$E_i$	$E_2$	$i_{\gamma\gamma}$	$E_1$	$E_i$	$E_2$	$i_{\gamma\gamma}$
		2867.52	0.153 (12)	2604.00	2979.90 (29)	2938.42	0.060 ( 7)
		2806.27	0.116 ( 8)			2877.17	0.034 ( 8)
		2675.14	0.069 ( 6)	2597.00	2986.90 (90)	2914.00	0.025 ( 6)
		2601.92	0.030 ( 7)	2582.20	3001.70 (30)	3001.70	0.024 ( 6)
		2509.98	0.028 ( 5)			2898.97	0.025 ( 6)
2670.60	2913.30 (40)	2871.82	0.037 ( 7)	2577.30	3006.60 (15)	3006.60	0.070 ( 8)
		2606.22	0.043 ( 7)			2965.12	0.026 ( 7)
2665.90	2918.00 (31)	2918.00	0.021 ( 6)			2903.87	0.076 ( 8)
		2610.92	0.021 ( 6)			2772.74	0.016 ( 6)
2611.50	2972.40 (28)	2930.92	0.121 (10)	2573.50	3010.40(100)	3010.40	0.035 ( 8)
		2516.63	0.047 ( 6)			2937.50	0.042 ( 5)

Analysis of the experimental data requires transformation of the peak areas of the resolved cascades into absolute values (in % per decay). However, the direct solution of this problem using, e.g., the areas of the peaks in the sum coincident spectrum is impossible because of the uncontrollable conditions of the experiment. First of all, this is due to difficulties of determining the number of captures in the target and the absolute efficiency of registration of the cascade in the geometry of the experiment. This problem can be solved by the normalization of relative intensities to the absolute values  $A_{\gamma\gamma}$  calculated for the most intense cascades by the relation

$$A_{\gamma\gamma} = i_1 \times B_r, \quad (1)$$

where the absolute intensities  $i_1$  of the primary transitions are taken from other works, and the branching ratios  $B_r$  are determined in a standard way from the codes of coincidences accumulated in this experiment.  $A_{\gamma\gamma}$  is the ratio between the intensity of a given cascade and total intensity of all cascades with  $E_1 + E_2 = const$ . The use of a maximally large ensemble of reference cascades in the normalization allows one to minimize both statistical and systematical errors of the procedure and practically reduce them to the errors of  $i_1$ .

Unfortunately, there are no reliable data on the absolute intensities of primary transitions for osmium isotopes under consideration. Therefore, we were forced to use the data [9] on relative intensities of  $\gamma$ -transitions following thermal neutron capture in  $^{190}\text{Os}$ . For their normalization, we measured the spectrum of  $\gamma$ -rays after thermal neutron capture in the target of natural Os and determined the ratios between the peak areas corresponding to  $\gamma$ -transitions with energies 7234, 7793( $^{190}\text{Os}$ ), 7835( $^{188}\text{Os}$ ) and 5147 keV ( $^{191}\text{Os}$ ). The absolute intensity of 5147 keV transition belonging to  $^{191}\text{Os}$  was determined to be equal  $I_1 = 14.4(14)\%$  per decay using the absolute intensities [10,11] of three other transitions, and data [5,12] on isotopic abundance and thermal neutron capture cross sections. This allowed us to transform the relative intensities of primary transitions in  $^{191}\text{Os}$  [9] into the absolute values and determine [13] the intensities of the two-step cascades in this nucleus. The coefficient of normalization of relative intensities of primary transitions in  $^{193}\text{Os}$  to absolute values was determined using the ratio of areas of the peaks corresponding to the cascades to the ground and to three low-lying levels of

TABLE 2. The sum energies  $E_c$  (in keV), the calculated  $I_{\gamma\gamma}^{\text{cal}}$  and experimental  $I_{\gamma\gamma}^{\text{exp}}$  intensities (% per decay) of the two-step cascades in  $^{193}\text{Os}$ .

$E_c$	$I_{\gamma\gamma}^{\text{exp}}$	$I_{\gamma\gamma}^{\text{cal}} [16,18]$	$I_{\gamma\gamma}^{\text{cal}} [17,18]$	$I_{\gamma\gamma}^{\text{cal}} [16,19]$	$I_{\gamma\gamma}^{\text{cal}} [17,19]$
5583.90	12.5(2)	6.2	6.5	4.7	5.3
5542.42	12.2(2)	5.6	5.7	4.4	4.7
5511.00	4.5(1)	2.9	3.0	2.2	2.5
5481.17	19.0(1)	5.1	5.3	4.0	4.4
5350.04	7.2 (2)	4.1	4.4	3.2	3.7
5288.22	3.9(2)	2.0	2.2	1.6	1.8
5276.82	8.1(4)	3.6	4.0	2.9	3.4
5184.88	4.0(2)	1.6	1.9	1.3	1.6
5128.13	3.8(2)	1.5	1.8	1.2	1.5
4874.70	1.5(1)	0.9	1.2	0.7	1.0
4694.42	3.4(2)	1.1	1.7	1.0	1.5
total	81(1)	34.6	37.7	27.2	31.4

*Note:* It was taken that in all variants of the calculation that the radiative strength function of M1 transitions does not depend on  $\gamma$ -quantum energy. The ratio of the widths of M1 transitions to that of E1 transitions at  $E_\gamma \approx B_n$  was taken equal to 0.15.

$^{191,193}\text{Os}$ , as well as the averaged efficiency of registration of the cascades over the corresponding spectra. It was determined to be 0.01077 for the relative intensities of the primary transitions from the data in Ref. [14].

The total absolute intensities  $I_{\gamma\gamma} = \sum i_{\gamma\gamma}$  of the cascades, with a fixed sum energy (including those unresolved experimentally), are given in Table 2. The data correspond to the energy detection threshold of 520 keV which was used to reject annihilation quanta. Nevertheless, the data are suitable for testing of the validity of level density and radiative strength function models in the excitation energy range almost up to  $B_n$ , as it is shown in Table 2.

### 3.1. Background cascades

Every spectrum – intensity distribution of the cascades with a given sum energy contains the following components: (i) the desired cascade both in form of pairs of resolved peaks and their superposition – continuous distribution of low amplitude (cascade energy is completely deposited in detectors); (ii) a “noise” line from registration of the part of the energy of quanta from cascades of higher energy.

On the average, the contribution of the latter in the spectrum practically equals zero, but in some local sections of the spectrum the distortions can be considerable. It should be noted that the main distortion is due to the cases of partial absorption of energy of one cascade transition in one detector and complete absorption of the energy of another transition in the other detector. Subtraction of this Compton background results in the appearance of characteristic symmetrical structures of variable sign in spectrum of cascades with smaller sum energy. As it was shown in

Ref. [8], these structures manifest themselves when the full energy peaks of high-energy cascades contain more than 1000 events. The use of the numerical algorithm for an improvement of the energy resolution [6] strengthens this effect. The shape of such structure is determined by the intensity of corresponding individual cascade of higher energy, choice of concrete windows “effect+background” and “background” (Fig. 1) and is due to the inevitable discrepancy in positions of these intervals. Of course, similar effect exists in the standard analysis of  $\gamma - \gamma$  coincidences, but there it is well “masked”.

Relatively precise and complete correction of the corresponding distortions in the spectra, from which the data of Fig. 2 were obtained, can be calculated. This requires the data on the probability of simultaneous registration of quanta  $E_1$  and  $E_2$  in the full energy peaks for all possible most intense cascades of higher energy (including cascades in other isotopes and elements situated in the neutron beam). This procedure is absolutely necessary if HPGe detectors with an efficiency of more than 25-30% are used in the experiment.

### 3.2. Contribution of $^{191}\text{Os}$

The contribution of  $^{191}\text{Os}$  appears, in particular, in the sum coincidence spectrum as overlapping of full energy peaks related with cascade transitions in  $^{193}\text{Os}$  and  $^{191}\text{Os}$ . As can be seen in Table 3, such overlapping affects 4 cascade intensity distributions measured in  $^{193}\text{Os}$ . It should be noted that this effect was taken into consideration only for the final levels of cascades with  $J_f \leq 5/2$  because, according to all previous experiments, the intensity of cascades which include just one quadrupole transition is considerably less than that of cascades with two dipole transitions.

*Table 3. The energies  $E_c$  and  $E_f$  (in keV) of the experimentally unresolved cascades and of the corresponding final levels, respectively, and the probable values of  $J^\pi$  in  $^{191,193}\text{Os}$ .*

$^{191}\text{Os}$			$^{193}\text{Os}$		
$E_c$	$E_f$	$J^\pi$	$E_c$	$E_f$	$J^\pi$
5485.9	273	5/2-	5481.2	103	3/2-
5287.0	472	5/2-	5288.2	296	5/2-
5184.5	574	1/2- 3/2-	5184.9	399	5/2-
5127.9	631	5/2-	5128.1	456	5/2-

The overlapping of peaks corresponding to different isotopes brings in the necessity to remove well separated, intense cascades belonging to the  $^{191}\text{Os}$  isotope from Table 1 and correct the data in Table 2 for their contribution. The correction has sense only if the cascades of  $^{193}\text{Os}$  determine a major part of the area of a given doublet in the sum coincidence spectrum. In this way, the experimentally resolved cascades of  $^{191}\text{Os}$  have been removed from all 4 spectra.

The removed cascades are attributed to  $^{191}\text{Os}$  if they were found within the limits of three standard errors of determination of the intermediate level or of  $\gamma$ -transition energy, and:

- (a) intermediate levels with a corresponding energy are not observed in other 7 spectra of  $^{193}\text{Os}$ ; but
- (b) the  $\gamma$ -transition with a close energy is observed in the cascade primary transitions of  $^{191}\text{Os}$ .

Of course, this procedure does not guarantee an absolute confidence in the results. It is, however, more suitable for the determination of level energies than for the determination of decay modes of excited states. A number of cascade transitions observed with a relatively large mean error of determination of their energies ( $\Delta E = 0.36$  keV) does not allow to suggest a more reliable method to exclude cascades belonging to  $^{191}\text{Os}$ . Moreover, presently available [15] information on thermal neutron radiative capture spectra of  $^{190,192}\text{Os}$  is considerably poorer than the data obtained in the reported experiment and cannot be used to solve the problem under consideration.

Correction of the total cascade intensities (Table 2) for the contribution of  $^{191}\text{Os}$  can be done in a simpler way. An analysis shows that the low-lying levels of  $^{191,193}\text{Os}$  with equal  $J_f^\pi$  and the same structure are populated by two-step cascades with approximately equal probabilities. It should be noted that approximative equality of intensities is observed also for the cascades terminating at the levels with different spins  $J = 1/2$  or  $3/2$ , but equal parity. Therefore, the ratio between the contributions of two isotopes in the case of such  $J_f^\pi$  was taken equal to the ratio between the number of neutron captures in  $^{190}\text{Os}$  and  $^{192}\text{Os}$ . Besides, the intensity of cascades terminating at the  $J_f^\pi = 5/2^-$  level of  $^{193}\text{Os}$  was assumed to be two times less than the cascade intensity to the  $J = 1/2, 3/2$  final levels of  $^{191}\text{Os}$  under conditions of equality of numbers of neutron captures in both isotopes.

The results of the procedure are taken into account in the data listed in Table 2. Certainly, it is an approximate solution of the problem. However, the unresolved doublets represent an insignificant part of the total cascade intensity. Hence, one may expect negligible influence of the corresponding error on the final results.

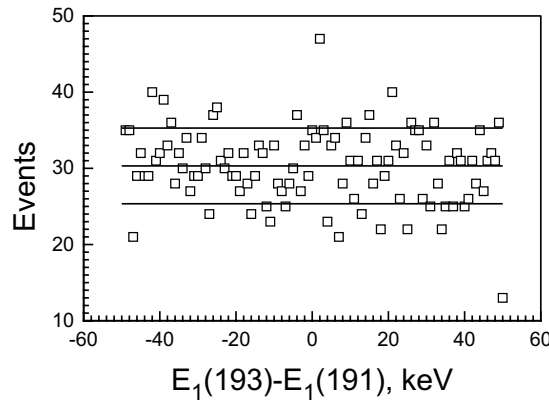


*Fig. 3. Frequency distribution of differences of the primary transition energies  $E_1$  of the cascades in  $^{193}\text{Os}$  and  $^{191}\text{Os}$  [13]. Horizontal lines represent the average value and mean-square deviation from it.*

The maximum number of primary transitions belonging to  $^{191}\text{Os}$  (included in Table 1) can be estimated from the frequency distribution of the differences between the energies of the primary transitions in the corresponding spectroscopic data. Such a frequency distribution for 1 keV energy bins in  $^{191,193}\text{Os}$  is shown in Fig. 3. The enhanced (as compared with neighbouring intervals) frequency of observation of the primary transitions with close energy can testify the admixture of the cascades of  $^{191}\text{Os}$  in Table 1. Mistaken isotopic identification is observed, probably, for 39(16) transitions among more than 500 primary transitions measured in the two isotopes. (Small but statistically significant deviation of the data given in Fig. 3 from zero can be related to the error in the energy calibration for different Os isotopes). There is a rather clear demonstration of reliability of the spectroscopic data obtained in our experiment.

### 3.3. Comparison with a known decay scheme

Investigation of the cascade  $\gamma$ -decay of heavy compound nuclei is a sensitive tool for obtaining spectroscopic information and reliable establishing of a decay scheme up to the excitation energy from 3 to 4 MeV. The confidence of observation of nuclear excited states is mainly determined by the intensity of populating cascades and depends weakly on the excitation energy. For these reasons, the decay scheme of  $^{193}\text{Os}$  above about 1 MeV established in our experiment seems to be more precise and reliable than those obtained earlier.

All levels of  $^{193}\text{Os}$  with  $J < 5/2$  observed in our measurements are listed in Table 1. The known decay scheme of this nucleus includes only a part of possible levels from those listed in Table 1. This is due to its construction mainly on the basis of spectra of the primary  $\gamma$ -transitions following thermal neutron radiative capture. However, these spectra were measured at the real detection threshold  $L_c \simeq 5 \times 10^{-3}$  events per decay. In our experiment, the states of  $^{193}\text{Os}$  populated by the cascades with the sum intensity exceeding  $2 - 4 \times 10^{-4}$  events per decay were observed. The energy of intermediate levels for the majority of these cascades was determined according to Ref. [8] reliably enough, too. In the case of the low intensity cascades, quanta ordering was determined [7] only for a part of them. Some of the cascades were observed only in one of 11 distributions and one cannot exclude that, possibly, some of the cascades listed in Table 1 can have the low-energy primary and high-energy secondary transitions.

## 4. Probable dominant component of the wave functions of the intermediate levels of most intense cascades

According to the modern theoretical notions, the wave function structure of any excited state is determined by a co-existence and interaction between the fermion (quasiparticles) and boson (phonons) excitations. As the excitation energy increases, a nucleus changes from practically mono-component excitations of

the mentioned types to the mixed (quasiparticle  $\otimes$  phonon) states with rather different [20] degrees of their fragmentation. This process should be investigated in details, but there are no adequate experimental methods to study the structure of the wave functions above the excitation energy of 1–3 MeV.

Nevertheless, some information on the probable dominant components of the wave functions of heavy deformed nuclei can be obtained. The authors of Ref. [21] suggested the search for the regularity in the excitation spectra of the intermediate levels of most intense cascades by means of the auto-correlation analysis of the smoothed distributions of the sum cascade intensities from Table 1. Intensities were smoothed by means of the Gaussian function  $F(E) = \sum_E I_{\gamma\gamma} \times \exp(-0.5(\Delta E/\sigma)^2)$ . The distribution of this type, smoothed with the parameter  $\sigma = 25$  keV, is given in Fig. 4 and the values of the auto-correlation function

$$A(T) = \sum_E F(E) \times F(E + T) \times F(E + 2T) \quad (2)$$

for different selection thresholds of the intense cascades are shown in Fig. 5. As was shown in Ref. [22], such an analysis cannot give a unique value of the equidis-

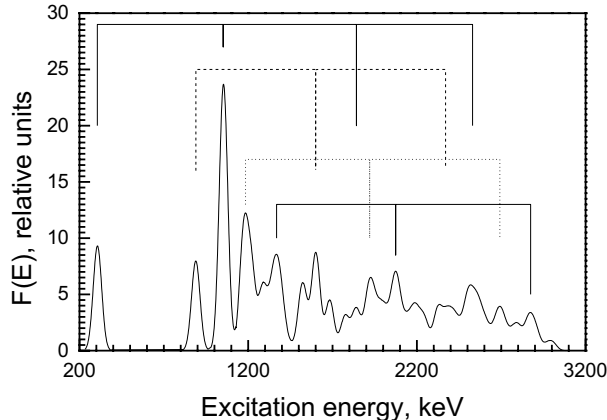


*Fig. 4. The dependence of the “smoothed” intensities of resolved cascades listed in Table 1 on the excitation energy. Possible “bands” of practically harmonic excitations of the nucleus are marked. The parameter  $\sigma = 25$  keV was used.*

tant period  $T$  even for the simulated spectra (for example, for 25 “bands” consisting from 4 levels with slightly distorted equidistant period) and provide estimation of the confidence level of the observed effect. In principle, both problems can be solved in experiments studying the two-step cascades in different resonances of the same nucleus. But some arguments to the state that the regularity really exists can be obtained from a comparison of the most probable equidistant periods in different nuclei. The set of the probable equidistant periods obtained so far (Fig. 6) allows for an assumption that the  $T$  value is approximately proportional to the number

of boson pairs of the unfilled nuclear shells. This allows one to consider the effect at the level of working hypothesis.

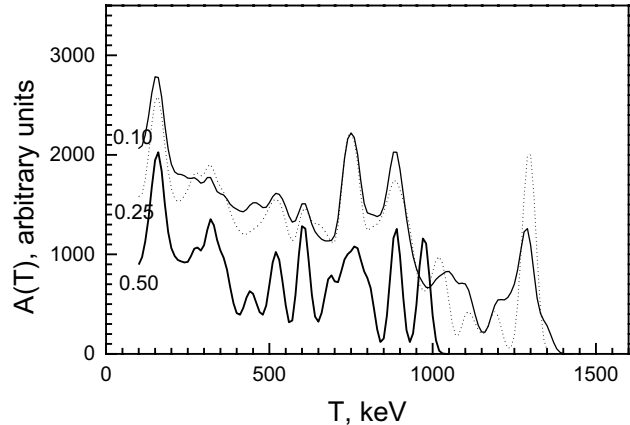


*Fig. 5. The values of the functional  $A(T)$  for three registration thresholds of most intense cascades. The value of the registration threshold (% per decay) is given in the figure.*

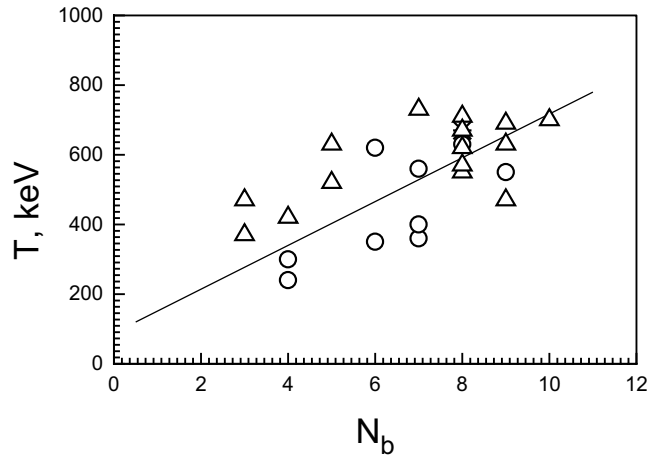


*Fig. 6. The value of the equidistant period  $T$  for  $^{193}\text{Os}$  (asterisk), even-odd (triangles) and odd-odd (circles) nuclei as a function of the number of boson pairs,  $N_b$ , in unfilled shells. The line represents possible dependence (drawn by eye).*

The regularity in the excitation spectra testifies to the harmonic nuclear vibrations. Thus, one can assume that the structure of the intermediate levels of the studied cascades contains considerable components of the rather weakly fragmented states like multi-quasiparticle excitations  $\otimes$  phonon or several phonons. This provides a logical explanation of the prominent decrease in the observed level density as compared with the predictions of the non-interacting Fermi-gas model: nuclear

excitation energy concentrates on phonos, and quasiparticles up to about 2 MeV are populated weakly or very weakly due to an insufficiency of energy for breaking up of nucleon pairs.

### 5. Conclusion

Information on the two-step  $\gamma$ -cascades, for a number of nuclei in the mass range  $114 \leq A \leq 200$  (see, for example, [23]) from thermal neutron capture experiments, forms a basis for the study of characteristics of the  $\gamma$ -decay process.

The results indicate the necessity to modify the model assumptions on the properties of the excited states of heavy nuclei. The obtained information demonstrates that a more correct description of the process under study requires more detailed accounting for a co-existence and interaction of the superfluid and normal phases of nuclear matter by the nuclear models. It appears impossible to achieve a complete correspondence between the observed and calculated parameters of nuclear reactions, for instance, the neutron-induced reaction. This concerns, partially, the total radiative widths of neutron resonances and the  $\gamma$ -spectrum.

#### *Acknowledgements*

This work was supported by GACR under contract No. 202/97/K038 and by RFBR Grant No. 99-02-17863.

#### References

- [1] S. T. Boneva, E. V. Vasilieva, Yu. P. Popov, A. M. Sukhovoij and V. A. Khitrov, Sov. J. Part. Nucl. **22(2)** (1991) 232.
- [2] S. T. Boneva et al., Part. Nucl. **22(6)** (1991) 698.
- [3] E. P. Grigoriev, V. A. Khitrov, A. M. Sukhovoij and E. V. Vasilieva Fizika B (Zagreb) **9(4)** (2000) 147.
- [4] J. Honzátko et al., Nucl. Instr. and Meth. A **376** (1996) 434.
- [5] F. D. Corte and A. Simonits, in *Proc. Int. Conf. on Nuclear Data for Science and Technology*, Mito, (1988), ed. S. Igarasi, Japan Atomic Energy Research Institute (1988) 583.
- [6] A. M. Sukhovoij and V. A. Khitrov, Sov. J. Prib. Tekhn. Eksp. **5** (1984) 27.
- [7] Yu. P. Popov, A. M. Sukhovoij, V. A. Khitrov and Yu. S. Yazvitsky, Izv. AN SSSR, Ser. Fiz. **48** (1984) 891.
- [8] S. T. Boneva, E. N. Vasilieva and A. M. Sukhovoij, Izv. RAN., Ser. Fiz., **51(11)** (1989) 2023.
- [9] E. Browne, Nuclear Data Sheets **V.56** (1989) 709.
- [10] P. Fettweis and J. C. Dehaes, Z. Phys. **314** (1983) 159.
- [11] R. F. Casten et al., Nucl. Phys. A **316** (1979) 61.
- [12] S. F. Mughabghab, *Neutron Cross Sections. Part B*, Academic Press, New York (1984).

- [13] V. A. Bondarenko, V. A. Khitrov, A. M. Sukhovoj, J. Honzátko and I. Tomandl, JINR preprint E3-99-343, Dubna (1999).
- [14] D. Benson, Jr., P. Kleinheinz, R. K. Sheline and E. B. Shera, Z. Phys. A **285** (1978) 405.
- [15] <http://www.nndc.bnl.gov/wallet/tnc/capgam.shtml>.
- [16] W. Dilg, W. Schantl, H. Vonach and M. Uhl, Nucl. Phys. A **217** (1973) 269.
- [17] A. V. Ignatyuk, *Proc. IAEA Consultants Meeting on the Use of Nuclear Theory and Neutron Nuclear Data Evaluation*, Trieste (1975) IAEA-190, Vol. 1, (1976) 211.
- [18] P. Axel, Phys. Rev. **126** (1962) 683.
- [19] S. G. Kadomenskij, V. P. Markushev and W. I. Furman, Yad. Fiz. **37** (1983) 165.
- [20] L. A. Malov and V. G. Soloviev, Yad. Fiz. **26**(4) (1977) 729.
- [21] A. M. Sukhovoj and V. A. Khitrov, Izv. RAN, Ser. Fiz. **61**(11) (1997) 2068.
- [22] E. V. Vasilieva et al., Bulletin of the Russian Acad. Science, Physics **57** (1993) 1582.
- [23] S. T. Boneva et al., Phys. At. Nuclei **62**(5) (1999) 832.

KASKADNI  $\gamma$ -RASPAD SLOŽENE JEZGRE  $^{193}\text{Os}$  I NEKI IZGLEDI  
DINAMIKE PROMJENA NUKLEARNIH OSOBINA ISPOD  $B_n$

Mjerili smo  $\gamma - \gamma$  kaskade u reakciji  $^{192}\text{Os}(n_{th}, \gamma)^{193}\text{Os}$  sudesnom metodom s dvama Ge detektorima. Utvrdili smo shemu raspada  $^{193}\text{Os}$  do uzbudne energije  $\sim 3$  MeV. Našli smo da je spektar viših međustanja najintenzivnijih kaskada gotovo harmoničan.